INTERNATIONAL JOURNAL OF HYDROGEN ENERGY 39 (2014) 8780–8790

Available online at www.sciencedirect.com

ScienceDirect

journal homepage: www.elsevier.com/locate/he

# Bonding in $PdH_2$ and $Pd_2H_2$ systems adsorbed on carbon nanotubes: Implications for hydrogen storage

*Ignacio López-Corral* [a], *Beatriz Irigoyen* [b], *Alfredo Juan* [c,*]

[a] *Instituto de Química del Sur (UNS-CONICET), Departamento de Química, Universidad Nacional del Sur, Av. Alem 1253, B8000CPB Bahía Blanca, Argentina*

[b] *Departamento de Ingeniería Química, Universidad de Buenos Aires, Facultad de Ingeniería, Pabellón de Industrias, Ciudad Universitaria, C1428EGA Ciudad Autónoma de Buenos Aires, Argentina*

[c] *Instituto de Física del Sur (UNS-CONICET), Departamento de Física, Universidad Nacional del Sur, Av. Alem 1253, B8000CPB Bahía Blanca, Argentina*

ARTICLE INFO

*Article history:*
Received 16 October 2013
Accepted 5 December 2013
Available online 2 January 2014

*Keywords:*
Hydrogen storage
Carbon nanotubes
Palladium
Clustering
DFT
Bonding

ABSTRACT

This work presents a bonding study of hydrogen adsorption processes on palladium decorated carbon nanotubes by using the density functional theory (DFT). First, we considered simple decoration models involving single palladium atoms or palladium dimers, and then we analyzed the adsorption of several molecular and dissociated hydrogen coordination structures, including Kubas-type complexes. In all cases we computed the energy, bonding and electronic structure for the different nanotube-supported hydrogen –palladium systems. Our results show that $Pd(H_2)$ and $Pd_2(H_2)$ complexes with relaxed but not dissociated H–H bonds are the most stable adsorbed systems. The role of *s*, *p* and *d* orbitals on the bonding mechanism for all adsorbates and substrates was also addressed. We found intermolecular donor–acceptor C–Pd and Pd–H delocalizations after adsorption. We also studied the palladium clustering effect on the hydrogen uptake based on Kubas-type bonding.



## 1. Introduction

Carbon nanotubes (CNTs) are considered one of the most promising materials for hydrogen storage due to their high surface-to-volume ratio, light weight and high stability. Weak dispersion forces are developed between physisorbed hydrogen molecules and bared CNTs, so the hydrogen storage capacity is not significant at room temperature and moderate pressures [1]. However, both experimental and theoretical studies have showed that CNTs and other carbonaceous materials become more active for hydrogen adsorption at ambient conditions when transition metal atoms are pre-adsorbed. The enhanced storage capacity has been ascribed to two mechanisms: the so-called spillover process and the Kubas bonding. The first mechanism involves different steps [2]: dihydrogen dissociation on the metallic decoration, followed by migration of hydrogen atoms through the metal particles and subsequent diffusion on the carbon surface. Experimental research suggests that the spillover plays a very

* *Corresponding author*. Fax: +54 291 4595142.
E-mail address: cajuan@uns.edu.ar (A. Juan).

0360-3199/$ – see front matter 
http://dx.doi.org/10.1016/j.ijhydene.2013.12.032

important role in the enhanced hydrogen uptakes observed in decorated carbon materials [3–7].

The second mechanism, known as Kubas-type bonding [8], is based on σ-bonding between one or more hydrogen molecules and *d* orbitals of transition metal atoms. Experimental evidence of this type of bonding was reported for Ti metal–-ethylene complexes [9] and mesoporous Ti oxides [10]. Quantum mechanical calculations predict that single transition metal atoms stabilized on carbon surfaces can bind several $H_2$ molecules with binding energies of 0.2–1.0 eV per molecule [11–14]. Those energies, intermediate between physisorption and chemisorption values, are adequate for reversible operation at moderate conditions [15]. However, most transition metals adsorbed on carbon surfaces tend to form clusters rather than stay as individual atoms, because metal–metal bonds are stronger than carbon–metal interactions. As a consequence, interaction of hydrogen with single metal atoms is not favored and the storage capacity decreases [16,17]. The Kubas bonding seems to constitute a viable mechanism for hydrogen storage when carbon materials are decorated with highly dispersed nanoparticles. In effect, Contescu et al. [18,19] have proposed that the Kubas-type bonding occurs in parallel with the spillover and other hydrogen uptake mechanisms (physisorption, hydride formation) in Pd-modified activated carbon fibers with a large fraction of Pd (~18%) as isolated single atoms. Their experimental observations and modeling also suggest that, at low and medium pressures, the contribution of spillover to the excess uptake may be smaller than previously thought for this system. Therefore, the study of the interaction between hydrogen and small Pd clusters involving Kubas bonding on carbon surfaces is a very interesting topic.

In previous reports, we modeled the adsorption of the hydrogen molecule on graphene-supported single Pd atoms [20] and $Pd_2$ dimers [21], including several hydrogen coordination structures. We found that $Pd(H_2)$ and $Pd_2(H_2)$ Kubas-type complexes are stable systems onto the Pd-decorated graphene surface, but also a $(PdH)_2$ ring without H–H bond can be originated in presence of dihydrogen [21]. It is reasonable to expect that the adsorbate–substrate interactions developed on a plane graphene sheet can be altered when a curved carbon layer is considered. To the best of our knowledge, there are a few theoretical studies about hydrogen adsorption on Pd-doped CNTs. Dag et al. [12] and Xiao et al. [14] reported electronic structure calculations for $Pd(H_2)$ Kubas complexes supported on single-walled (SW) CNTs. In this paper we analyze several $PdH_2$ and $Pd_2H_2$ systems adsorbed on a SWCNT. The bonding evolution and atomic orbital contributions during the adsorption process were addressed in all cases.

## 2. Computational details and adsorption models

Spin-polarized density functional theory (DFT) calculations were performed using the SIESTA (Spanish Initiative for Electronic Simulations with Thousands of Atoms) code [22,23]. The exchange-correlation term was modeled with the generalized gradient approximation (GGA) parameterized by Perdew, Burke and Ernzerhof (PBE) [24]. We chose a double-ζ plus polarization (DZP) basis sets, which usually represents a good balance between well converged results and a reasonable computational cost [23,25]. An energy shift of 50 meV was selected in order to limit the range of the basis pseudo-atomic orbitals. Standard norm-conserving Troullier–Martins pseudopotentials were used to model the core electrons of C, Pd and H [26]. The charge density was projected onto a real-space grid with an energy cutoff of 150 Ry [22]. The equilibrium geometries were fully relaxed by the conjugate gradient (CG) method. Once the optimized adsorption geometries were obtained, the evolution of chemical bonding during the different adsorption processes was studied. We computed overlap population (OP) belonging to atom pairs in the preferential adsorption geometries. An OP value constitutes a measure of the bonding between two selected atoms [27]. Mulliken atomic orbital population analysis was also carried out to determine which orbitals are the main contributors to the bonding between atoms. This computational procedure was used in our previous studies [20,21]. Comparative tests were performed with the YAEHMOP package [28,29].

We selected a (8,0) zigzag SWCNT modeled by a $20 \times 8.52 \times 20$ Å$^3$ supercell containing 64 C atoms, with a double lattice parameter along the tube axis in order to reduce the adsorbate–adsorbate interaction (see Fig. 1a). A vacuum region of ~14 Å was taken along the other cell directions to avoid interactions between periodic images. The Brillouin zone was sampled in all cases by $1 \times 20 \times 1$ Monkhorst-Pack **k**-points [30]. First, we modeled the decoration of the (8,0) SWCNT adsorbing one Pd atom per unit cell on four possible high symmetry locations: the hollow site above a hexagon, the top site above a C atom, the regular bridge site above an axial C–C bond, and the zigzag bridge site above a C–C bond tilted to the tube axis. We found that the most preferable location of Pd is the regular bridge site (see Fig. 1b), so our further study was limited to this location. This result is consistent with previous DFT calculations [14,31,32]. We also considered the adsorption of a $Pd_2$ dimer on the SWCNT including two Pd atoms per unit cell. As suggested in the literature [33,34], we placed the $Pd_2$ system parallel to the carbon surface on regular bridge sites, which is the most stable configuration of the adsorbed dimer. Two $Pd_2$ adsorption geometries were analyzed, called configuration I and II. In the first the Pd atoms are positioned on second neighbor C–C bonds (Fig. 1c), while in the last the $Pd_2$ dimer is located perpendicular to the tube axis (Fig. 1d).

Following our previous studies about hydrogen adsorption on Pd-decorated graphene [20,21], four $PdH_2$ and three $Pd_2H_2$ complexes were considered (see Fig. 2). The $Pd(H_2)$ system A is the Kubas complex, with a relaxed H–H bond pointing towards the Pd atom. The linear Pd–H–H isomer B is also a dihydrogen complex, even though comes from an end-on approach mode. In contrast, complexes C and D have dissociated H–H bonds, but only the latter adopts a linear H–Pd–H configuration. On the other hand, the rhomboid $(PdH)_2$ structure E, which comes from a perpendicular interaction between $H_2$ and $Pd_2$, is the unique $Pd_2H_2$ system studied without H–H bond. Both the trapezoidal configuration F and the Kubas-type complex G have elongated but not dissociated H–H bonds. The calculated geometries, overlap populations and binding

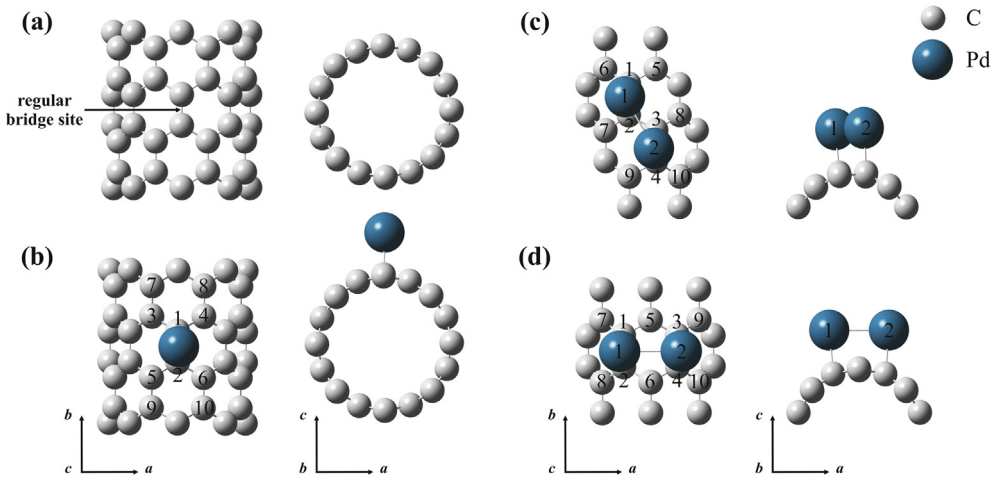


**Fig. 1 – (a) Unit cell of the (8,0) SWCNT system. The regular bridge site is indicated. (b) Pd/SWCNT system. (c) Configuration I of the $Pd_2$/SWCNT system. (d) Configuration II of the $Pd_2$/SWCNT system.**

energies of the considered $PdH_2$ and $Pd_2H_2$ systems, without a carbon support, are presented in Table 1. Isolated $H_2$ and $Pd_2$ molecules are also included. Our results are in good agreement with those reported in related DFT works [35,36]. Next, we examined the interaction of the $H_2$ molecule with the nanotube-supported single Pd atoms and $Pd_2$ dimers. Different adsorbed configurations were examined. According to previous theoretical calculations [12,14], we placed the $PdH_2$ systems in a normal plane to the carbon layer, with the hydrogen atoms arranged either along the tube axis or perpendicular to the tube axis. The $Pd_2H_2$ complexes were placed in a parallel or normal plane to the nanotube surface.

Finally, we calculated the binding energy per Pd atom, $E_b$(Pd), and the binding energy per $H_2$ molecule, $E_b(H_2)$, from the following expressions:

$$E_b(\mathrm{Pd}) = [E(\mathrm{SWCNT}) + n\,E(\mathrm{Pd}) - E(\mathrm{Pd}_n/\mathrm{SWCNT})]/n \quad (1)$$

$$E_b(\mathrm{H_2}) = E(\mathrm{Pd}_n/\mathrm{SWCNT}) + E(\mathrm{H_2}) - E(\mathrm{H_2}/\mathrm{Pd}_n/\mathrm{SWCNT}) \quad (2)$$

where $n$ is 1 or 2, according to the number of Pd atoms, and $E$(SWCNT), $E$(Pd), $E(H_2)$, $E(Pd_n/SWCNT)$ and $E(H_2/Pd_n/SWCNT)$ are the total energy of the bare SWCNT, the free Pd atom, the free $H_2$ molecule, the Pd-decorated SWCNT, and the $H_2$ molecule adsorbed on the Pd-decorated SWCNT. Therefore, a positive binding energy corresponds to an optimized stable structure.

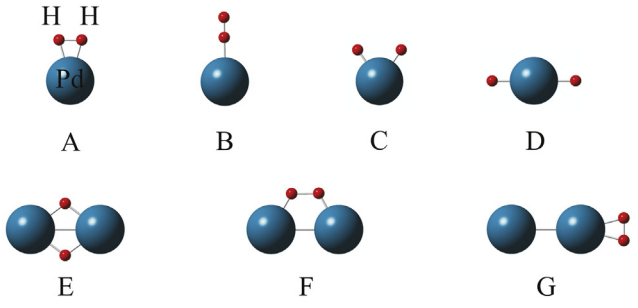


**Fig. 2 – Free $PdH_2$ (A to D) and $Pd_2H_2$ (E to G) systems. A and G are Kubas-type complexes.**

## 3. Results and discussions

### 3.1. *Pd/SWCNT and $Pd_2$/SWCNT systems*

We found that the most stable location of a single Pd atom on the SWCNT is above of a C–C bond parallel to the tube axis, with a C–Pd distance of 2.12 Å and a binding energy of 1.80 eV. Similar values were reported by Durgun et al. [31,32] and Xiao et al. [14]. The geometrical optimization and bonding results for the SWCNT decorated with individual Pd atoms on regular bridge sites are listed in Table 2. The atom labeling is presented in Fig. 1b. It can be seen that two new C–Pd bonds with important OP values are originated after Pd adsorption. At the same time, the C–C bonds nearby the decoration point are elongated and weakened. These changes decrease with the distance to the adsorption site. In effect, the C1–C2 bond, which constitutes the bridge site, is stretched 2.3% and its OP value decrease 5.8% when the Pd atom is adsorbed, but the C1–C3, C1–C4, C2–C5 and C2–C6 bonds are lengthened 1.4% and weakened 4.5%. Surface's bonds more distant to the adsorption position are almost not affected.

Table 2 also shows the atom–atom distances and OP values for the optimized SWCNT with $Pd_2$ dimers parallel to the carbon surface on regular bridge sites. The binding energies per Pd atom, calculated from Equation (1) with $n = 2$, are included in Table 2 for two considered configurations. Local adsorption geometries are presented in Fig. 1, indicating the atom numbering. $E_b$(Pd) for configuration I (Fig. 1c) is higher than that of the configuration II, in which the dimer is perpendicular to the tube axis (Fig. 1d). In the same way, C–Pd distances and OP values belonging to the configuration I are shorter and bigger, respectively, than those corresponding to configuration II. Simultaneously, the Pd–Pd bond is notoriously lengthened and weakened after the adsorption process.

**Table 1 – Distances (*d*), overlap populations (OP) and binding energies ($E_b$) for free $H_2$, $Pd_2$, $PdH_2$ and $Pd_2H_2$ systems.[a]**

| System | H–H bond | | Pd–H bond | | Pd–Pd bond | | $E_b$ (eV) |
|---|---|---|---|---|---|---|---|
| | *d* (Å) | OP | *d* (Å) | OP | *d* (Å) | OP | |
| $H_2$ | 0.750 (0.761) | 0.856 | – | – | – | – | 4.64 (4.66)[b] |
| $Pd_2$ | – | – | – | – | 2.548 (2.526) | 0.157 | 0.69 (0.83)[c] |
| $PdH_2$ A | 0.903 (0.883) | 0.673 | 1.689 (1.683) | 0.129 | – | – | 0.94 (0.84)[d] |
| $PdH_2$ B | 0.797 (0.797) | 0.794 | 1.747 (1.741) | 0.064 | – | – | 0.41 (0.46)[d] |
| $PdH_2$ C | – | – | 1.538 (1.520) | 0.483 | – | – | 0.76 (0.64)[d] |
| $PdH_2$ D | – | – | 1.661 (1.690) | 0.631 | – | – | Unstable |
| $Pd_2H_2$ E | – | – | 1.693 (1.674) | 0.309 | 2.716 (2.726) | 0.062 | 2.07 (2.07)[e] |
| $Pd_2H_2$ F | 1.060 (1.033) | 0.520 | 1.612 (1.602) | 0.226 | 2.649 (2.647) | 0.106 | 1.23 (1.29)[e] |
| $Pd_2H_2$ G | 0.875 (0.872) | 0.707 | 1.742 (1.700) | 0.104 | 2.705 (2.775) | 0.081 | 0.75 (0.71)[e] |

[a] DFT results of Efremenko et al. [34] are shown in parentheses.
[b] $E_b = 2E(H) - E(H_2)$.
[c] $E_b = 2E(Pd) - E(Pd_2)$.
[d] $E_b = E(H_2) + E(Pd) - E(PdH_2)$
[e] $E_b = E(H_2) + E(Pd_2) - E(Pd_2H_2)$.

The interatomic distance and OP value for the unsupported $Pd_2$ system is 2.548 Å and 0.157, respectively (see Table 1). Table 2 reveals that the elongation and weakening of the Pd–Pd interaction for configuration II (12.1% and 50.9% respectively) are bigger than those for configuration I (8.7% and 27.3% respectively). Therefore, we can consider that the adsorbed dimer is less stable when it adopts configuration II. C–C bonds nearby bridge sites are also elongated and weakened during $Pd_2$ adsorption. These changes are more important for configuration I. The C2–C3 bond, which connects the two C–C bonds with C atoms directly bonded to the dimer in configuration I, is the weakest surface's bond after the decoration process. All these findings indicate that configuration I originates stronger C–Pd interactions, so we can conclude that the adsorption of two Pd atoms on second neighbor C–C bonds is the preferential interaction mode between $Pd_2$ and SWCNT.

The binding energy obtained for the Pd adsorption on the regular bridge site of the SWCNT is approximately 40% bigger than those reported for the C–C site of a Pd-decorated graphene sheet ($E_b$(Pd) = 1.08 eV [20]). These energy values show that bonding of individual Pd atoms is stronger on a nanotube surface than on a graphene monolayer. As a consequence, we can predict that the finite curvature makes the CNTs more reactive. A similar conclusion was previously presented by Maiti and Ricca [37]. On the other hand, if we compare the energy values corresponding to the Pd/SWCNT and $Pd_2$/SWCNT systems, it is possible to observe that the dimer adsorption in configuration I is only 0.15 eV/Pd more stable than the adsorption of individual Pd atoms on distant sites of the nanotube. In case of configuration II, the dimer presents the same stability as the individual Pd atoms. In a previous work [21], we found that the parallel approach of $Pd_2$ to second neighbor bridge sites on a graphene sheet is 0.24 eV/Pd more

**Table 2 – Distances (*d*), overlap populations (OP) and binding energies ($E_b$) for optimized Pd/SWCNT and $Pd_2$/SWCNT systems.[a]**

| Pd/SWCNT (regular bridge site) | | | $Pd_2$/SWCNT (configuration I) | | | $Pd_2$/SWCNT (configuration II) | | |
|---|---|---|---|---|---|---|---|---|
| $E_b$(Pd) = 1.80 eV/Pd | | | $E_b$(Pd) = 1.96 eV/Pd | | | $E_b$(Pd) = 1.80 eV/Pd | | |
| Bond | *d* (Å) | OP | Bond | *d* (Å) | OP | Bond | *d* (Å) | OP |
| C1–C2 | 1.453 | 0.966 | C1–C2 | 1.450 | 0.970 | C1–C2 | 1.447 | 0.971 |
| C1–C3 | 1.457 | 0.935 | C3–C4 | 1.446 | 0.977 | C3–C4 | 1.447 | 0.971 |
| C1–C4 | 1.457 | 0.934 | C2–C3 | 1.482 | 0.895 | C1–C5 | 1.457 | 0.941 |
| C2–C5 | 1.457 | 0.935 | C1–C5 | 1.455 | 0.932 | C2–C6 | 1.457 | 0.942 |
| C2–C6 | 1.457 | 0.934 | C1–C6 | 1.453 | 0.940 | C3–C5 | 1.457 | 0.941 |
| C3–C7 | 1.416 | 1.037 | C2–C7 | 1.455 | 0.949 | C4–C6 | 1.457 | 0.942 |
| C4–C8 | 1.417 | 1.036 | C3–C8 | 1.453 | 0.954 | C1–C7 | 1.446 | 0.954 |
| C5–C9 | 1.416 | 1.038 | C4–C9 | 1.456 | 0.930 | C2–C8 | 1.446 | 0.954 |
| C6–C10 | 1.416 | 1.037 | C4–C10 | 1.453 | 0.941 | C3–C9 | 1.446 | 0.955 |
| – | – | – | – | – | – | C4–C10 | 1.446 | 0.955 |
| C1–Pd | 2.122 | 0.158 | C1–Pd1 | 2.139 | 0.159 | C1–Pd1 | 2.195 | 0.127 |
| C2–Pd | 2.120 | 0.159 | C2–Pd1 | 2.187 | 0.141 | C2–Pd1 | 2.195 | 0.127 |
| – | – | – | C3–Pd2 | 2.233 | 0.129 | C3–Pd2 | 2.197 | 0.126 |
| – | – | – | C4–Pd2 | 2.175 | 0.149 | C4–Pd2 | 2.197 | 0.127 |
| – | – | – | Pd1–Pd2 | 2.769 | 0.114 | Pd1–Pd2 | 2.857 | 0.077 |

[a] Binding energies were calculated according Eq. (1). Atom labeling is indicated in Fig. 1.

stable than the adsorption of single Pd atoms. These results indicate that the interaction between $Pd_2$ and SWCNT is smaller than that obtained on a flat graphene layer. Therefore, the dimerization process seems be even less important on the SWCNT. This behavior can be attributed to the higher reactivity of the curved carbon surface, which improves the C–Pd interactions and facilitates the atomization of the palladium decoration. The same considerations are valid for Pd-modified activated carbon [38]. On the contrary, previous theoretical works showed that carbon-supported open-shell transition metals, like Ti [16] and Sc [17], have a stronger preference to form clusters. Taking into consideration high surface area of carbon materials, it is possible to expect that in real carbon supports with low palladium loading a significant part of metal nanoparticles exists in the atomically dispersed form. A recent scanning transmission electron microscopy study [19] provides positive identification of isolated Pd atoms stabilized in the structure of activated carbon fibers, with an 18 wt % of the total Pd content dispersed as single atoms throughout the volume of the carbon matrix.

Finally, we evaluated atomic orbital occupations in the optimized Pd/SWCNT system, using the Mulliken population analysis. Our results are listed in Table 3 according the atom labeling indicated in Fig. 1b. It can be seen that, with respect to the $5s^0 5p^0 4d^{10}$ configuration in the free Pd atom, the Pd 4*d* orbitals transfer electron density towards the nearest C atoms, while the Pd 5*s* orbital receives charge from the support. The electronic configuration of the C1 and C2 atoms is $2s^{1.171} 2p^{2.823}$ in the bare SWCNT without Pd. Table 3 shows that Pd adsorption on the C1–C2 bond increases 2.6% the electron occupation of the 2*s* orbitals of C1 and C2 atoms, and diminishes 2.9% the occupancy of the 2*p* states of these atoms. C atoms away from the decoration point show almost no changes in their electron orbital occupations. Thus, the C–Pd overlap is characterized in this system by two coupled intermolecular donor–acceptor delocalizations: donation of palladium towards the surface and back-donation in the reverse direction. A similar interpretation has been presented for small palladium clusters adsorbed on activated carbon [38]. This bonding mechanism is analogous to that observed in the Pd/graphene system [20], but the back-donation to Pd 5*s* orbitals is much more pronounced on graphene. In contrast, the Pd 4*d* to SWCNT donation is as significant as the back-donation, and the C–Pd interaction results stronger on the curved carbon surface. Table 3 also shows the electron orbital populations in the $Pd_2$/SWCNT systems considered (Fig. 1c and d). The electronic configuration in the isolated $Pd_2$ dimer is $5s^{0.090} 5p^{0.027} 4d^{9.883}$. Both the Pd 4*d* to C 2*s* donation and the C 2*p* to Pd 5*s* back-donation are present in the two systems. However, configuration I involves more important donor–acceptor charge transfer between $Pd_2$ and SWCNT, leading to stronger C–Pd bonds. Our previous DFT calculations conclude that the adsorption of $Pd_2$ on graphene is accompanied by a significant back-donation, and in consequence the C–Pd OP values are smaller on that flat support [21].

### 3.2. $H_2$/Pd/SWCNT systems

We considered the adsorption of the four $PdH_2$ systems shown in Fig. 2 (A to D) on regular bridge sites of the SWCNT. Two initial adsorbed orientations were tested for each complex, with the hydrogen atoms arranged either along the tube axis or perpendicular to the tube axis as indicated in Fig. 3. The relevant distances and overlap populations are presented in Table 4 (see atom numbering in Fig. 3). The binding energies per $H_2$ molecule, $E_b(H_2)$, were calculated from Equation (2) with $n = 1$. The preferential carbon-supported $PdH_2$ system is the complex A perpendicular to the tube axis (Fig. 3h), with a binding energy of $E_b(H_2) = 0.66$ eV. The other orientation of this complex, with the H–H bond along the tube axis (Fig. 3i), is 72 meV less stable. Although in these configurations the H–H bond is relaxed due to the Kubas bonding, the $H_2$ molecule is not dissociated. The adsorption of the terminal Pd–H–H isomer B (Fig. 3j) is also possible, but leads to a much lower $E_b(H_2)$. In contrast, we found that the system C, which is the second most stable unsupported geometry (see Table 1), is unstable on the nanotube and relaxes to the Kubas complex with a very similar $E_b(H_2)$ value. Finally, the linear H–Pd–H approach mode D is not stable on the carbon surface (Fig. 3k and l). Our results indicate that only the adsorption of $Pd(H_2)$ dihydrogen complexes is feasible on the SWCNT, whereas classic hydrides without H–H bond are unstable.

**Table 3 – Electron orbital occupations for optimized Pd/SWCNT and $Pd_2$/SWCNT systems.[a]**

| Atom | Pd/SWCNT (regular bridge site) | | | $Pd_2$/SWCNT (configuration I) | | | $Pd_2$/SWCNT (configuration II) | | |
|---|---|---|---|---|---|---|---|---|---|
| | *s* | *p* | *d* | *s* | *p* | *d* | *s* | *p* | *d* |
| C1 | 1.201 | 2.742 | – | 1.198 | 2.740 | – | 1.195 | 2.739 | – |
| C2 | 1.201 | 2.742 | – | 1.205 | 2.718 | – | 1.195 | 2.742 | – |
| C3 | 1.176 | 2.815 | – | 1.203 | 2.721 | – | 1.195 | 2.739 | – |
| C4 | 1.177 | 2.812 | – | 1.196 | 2.740 | – | 1.195 | 2.742 | – |
| C5 | 1.176 | 2.815 | – | 1.177 | 2.805 | – | 1.186 | 2.767 | – |
| C6 | 1.177 | 2.812 | – | 1.175 | 2.818 | – | 1.186 | 2.757 | – |
| C7 | 1.171 | 2.826 | – | 1.173 | 2.821 | – | 1.173 | 2.827 | – |
| C8 | 1.171 | 2.827 | – | 1.173 | 2.823 | – | 1.173 | 2.816 | – |
| C9 | 1.171 | 2.826 | – | 1.178 | 2.790 | – | 1.173 | 2.827 | – |
| C10 | 1.171 | 2.827 | – | 1.174 | 2.814 | – | 1.173 | 2.816 | – |
| Pd1 | 0.358 | 0.026 | 9.826 | 0.377 | 0.053 | 9.790 | 0.320 | 0.062 | 9.821 |
| Pd2 | – | – | – | 0.361 | 0.059 | 9.806 | 0.319 | 0.062 | 9.822 |

[a] Atom labeling is indicated in Fig. 1.

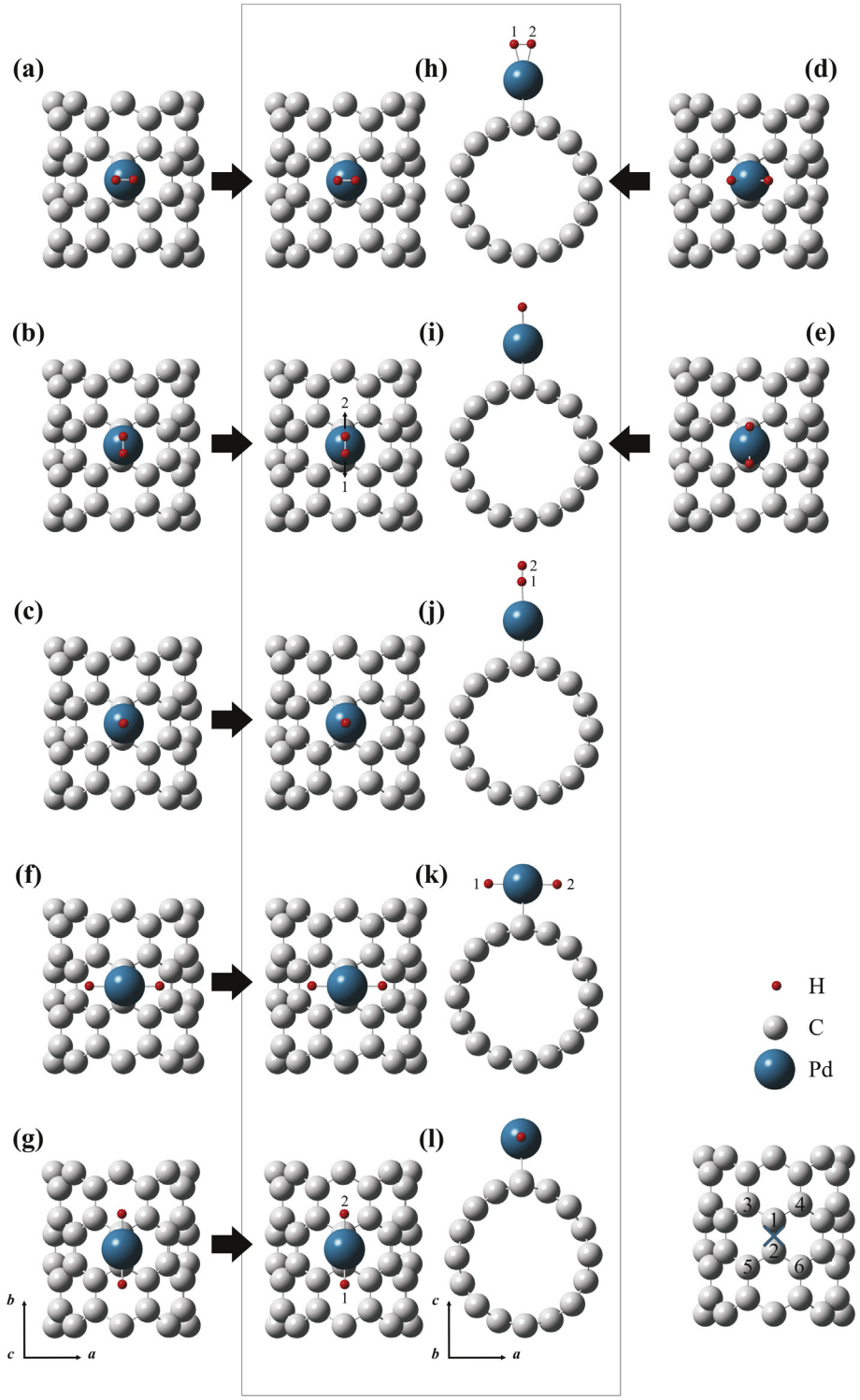


**Fig. 3 – Initial adsorption geometries for the $H_2$/Pd/SWCNT systems. (a) Complex A perpendicular to the tube axis. (b) Complex A along the tube axis. (c) Complex B. (d) Complex C perpendicular to the tube axis. (e) Complex C along the tube axis. (f) Complex D perpendicular to the tube axis. (g) Complex D along the tube axis. Final adsorption geometries (h to l) are also indicated.**

It can be seen from Tables 1and 4 that when the adsorption of the system A on the nanotube is perpendicular to the tube axis, the H–H distance in the free complex is decreased 8.1% and the corresponding OP value is increased 12.3%. Simultaneously, the Pd–H bonds are strongly elongated and weakened, until 6.3% and 44.1% respectively, due to the interaction between Pd($H_2$) and the support. On the other hand, C–Pd bonds are stretched 1.6% after $H_2$ adsorption on

**Table 4 – Distances ($d$), overlap populations (OP) and binding energies ($E_b$) for optimized $H_2$/Pd/SWCNT systems.[a]**

| Bond | $H_2$/Pd/SWCNT A (perpendicular to the tube axis) | | $H_2$/Pd/SWCNT A (along the tube axis) | | $H_2$/Pd/SWCNT B | |
|---|---|---|---|---|---|---|
| | $E_b(H_2) = 0.63$ eV | | $E_b(H_2) = 0.56$ eV | | $E_b(H_2) = 0.22$ eV | |
| | $d$ (Å) | OP | $d$ (Å) | OP | $d$ (Å) | OP |
| C1–C2 | 1.442 | 0.990 | 1.440 | 0.989 | 1.450 | 0.975 |
| C1–C3 | 1.454 | 0.942 | 1.450 | 0.948 | 1.456 | 0.937 |
| C1–C4 | 1.454 | 0.942 | 1.451 | 0.947 | 1.457 | 0.936 |
| C2–C5 | 1.454 | 0.941 | 1.451 | 0.947 | 1.456 | 0.937 |
| C2–C6 | 1.454 | 0.941 | 1.451 | 0.947 | 1.457 | 0.936 |
| C1–Pd | 2.156 | 0.137 | 2.172 | 0.132 | 2.136 | 0.149 |
| C2–Pd | 2.154 | 0.138 | 2.169 | 0.133 | 2.134 | 0.150 |
| Pd–H1 | 1.790 | 0.073 | 1.808 | 0.068 | 1.877 | 0.033 |
| Pd–H2 | 1.795 | 0.072 | 1.808 | 0.069 | – | – |
| H1–H2 | 0.830 | 0.755 | 0.822 | 0.762 | 0.768 | 0.827 |

[a] Binding energies were calculated according Eq. (2) with $n = 1$. Atom labeling is indicated in Fig. 3.

the decoration, with a weakening of about 13.5% (compare Table 2 vs. Table 4). Notice that in presence of hydrogen C–Pd overlaps are still present, so we can deduce that the Kubas complex remains on the SWCNT. Nearby C–C overlaps are also affected: the C1–C2 bond is shortened 0.8% and its OP value increased 2.5%, while C1–C3, C1–C4, C2–C5 and C2–C6 bonds undergo small changes. The distortion of the surface's bonds away from the site bridge is almost negligible. Our calculated geometry and binding energy of the adsorbed Kubas complex are in good agreement with those reported in the literature [12,14].

Also from Table 4, very similar C–Pd and C–C OP values can be observed after adsorption of the system A along the tube axis. However, smaller Pd–H overlaps are obtained in this case and a stronger H–H bond is present. In summary, when the Kubas complex is formed on the Pd-decorated SWCNT new Pd–H bonds are originated, C–Pd interactions are weakened and consequently C–C bonds are strengthened. We found that the dihydrogen complex B presents an analogous behavior after adsorption on the nanotube surface, but the changes in the H–H, C–Pd and C–C OP values are smaller due to a much weaker Pd–H interaction (see Table 4). Although the $H_2$/Pd/SWCNT coordination structures here obtained are similar to those found on graphene [20], stronger C–Pd overlaps are produced on a curved carbon surface, as it was also indicated in the preceding section. As a consequence, the nanotube-supported $PdH_2$ systems have longer and weaker Pd–H bonds than those of the corresponding graphene-adsorbed complexes. Accordingly, higher binding energies were obtained for all complexes adsorbed on graphene (for example, $E_b(H_2) = 1.85$ eV for the Kubas complex [20]).

Table 5 lists the Mulliken orbital occupations for the optimized $H_2$/Pd/SWCNT systems A and B shown in Fig. 3. It can see that when the Kubas complex is adsorbed perpendicular to the nanotube axis, the electron occupations of C1 and C2 2$s$ orbitals decreased 0.2%, while the 2$p$ orbitals of these C atoms populate 0.9% (compare values in Tables 3 and 5). C orbitals more distant to the bridge site are less influenced. The electron occupancies of C 2$s$ and 2$p$ orbitals also are diminished and increased, respectively, after the Pd($H_2$) Kubas bonding along the tube axis. The adsorbed complex B leads to smaller changes in the occupations of the C orbitals, because much weaker Pd–H interactions are developed in this case. Therefore, we can conclude that the adsorption of the $H_2$ molecule on the Pd-modified SWCNT is accompanied by a reduction of the C–Pd donation and back-donation interactions, which produces a weakening of the C–Pd overlap. Regarding H atoms, the H 1$s$ orbital occupancy is 0.943 in the unsupported Kubas complex, and 0.985 and 0.965 for H1 and H2 atoms, respectively, in the free Pd–H1–H2 system B. As can be seen from Table 5, the H 1$s$ orbitals of adsorbed $PdH_2$ complexes are

**Table 5 – Electron orbital occupations for optimized $H_2$/Pd/SWCNT systems.[a]**

| Atom | $H_2$/Pd/SWCNT A (perpendicular to the tube axis) | | | $H_2$/Pd/SWCNT A (along the tube axis) | | | $H_2$/Pd/SWCNT B | | |
|---|---|---|---|---|---|---|---|---|---|
| | $s$ | $p$ | $d$ | $s$ | $p$ | $d$ | $s$ | $p$ | $d$ |
| C1 | 1.198 | 2.767 | – | 1.196 | 2.765 | – | 1.201 | 2.754 | – |
| C2 | 1.199 | 2.767 | – | 1.196 | 2.765 | – | 1.201 | 2.753 | – |
| C3 | 1.176 | 2.816 | – | 1.176 | 2.816 | – | 1.176 | 2.815 | – |
| C4 | 1.176 | 2.814 | – | 1.176 | 2.814 | – | 1.176 | 2.813 | – |
| C5 | 1.176 | 2.816 | – | 1.176 | 2.816 | – | 1.176 | 2.815 | – |
| C6 | 1.176 | 2.814 | – | 1.176 | 2.813 | – | 1.177 | 2.813 | – |
| Pd | 0.378 | 0.037 | 9.784 | 0.372 | 0.038 | 9.801 | 0.359 | 0.021 | 9.818 |
| H1 | 0.967 | – | – | 0.969 | – | – | 0.991 | – | – |
| H2 | 0.968 | – | – | 0.969 | – | – | 0.987 | – | – |

[a] Atom labeling is indicated in Fig. 3.

more populated than in unsupported structures, since Pd atoms are involved in C–Pd interactions and the Pd–H bonds are weakened. We also found that the Pd 5s orbital undergoes an important increase in its electron occupation when the $H_2$ molecule is adsorbed, so the H(1s)–Pd(5s) interaction could be assumed as the main contribution to the Pd–H overlap. A similar orbital bonding scheme was also observed for dihydrogen adsorption on Pd-decorated graphene [20].

Finally, we focused on the Kubas-type bonding between $H_2$ and the Pd atom adsorbed on the SWCNT. The Kubas coordination can be interpreted by means of two cooperative donor–acceptor delocalizations [8]: $\sigma$ donation from $H_2$ $\sigma$ orbital to the Pd 5s orbital, and the $\pi$ back-donation from Pd 4*d* orbitals to the $H_2$ $\sigma^*$ orbital. Our calculations show that the electron occupations of the $H_2$ $\sigma$ and $\sigma^*$ orbitals are 1.849 and 0.038, respectively, for the free system A. After Pd($H_2$) adsorption perpendicular to the nanotube axis, the occupancy of the $\sigma$ bonding orbital is increased to 1.914, while the $\sigma^*$ antibonding orbital is depopulated to 0.022. These results suggest that the presence of the SWCNT decreases both the $\sigma$ donation from the $H_2$ $\sigma$ orbital and the $\pi$ back-donation to the $H_2$ $\sigma^*$ orbital. As a consequence, the OP Pd–H and H–H values become smaller and higher, respectively, than those of the unsupported complex. The same behavior was found for the Kubas coordination along the tube axis. However, in these case the electron populations of the $H_2$ $\sigma$ and $\sigma^*$ orbitals are 1.917 and 0.020, respectively, so the $\sigma$ donation and the $\pi$ back-donation are smaller than those developed in the perpendicular Pd($H_2$) adsorption on the nanotube. All these observations are in line with our previous energetic and OP analysis. The Kubas complexes supported on a graphene layer lead to higher Pd–$H_2$ electron delocalizations, because the interaction between the adsorbed Pd atoms and a flat carbon surface is weaker than in a SWCNT [20].

### 3.3. *$H_2$/$Pd_2$/SWCNT systems*

We examined the adsorption on the SWCNT of the three $Pd_2H_2$ systems shown in Fig. 2 (E to G). In all cases the two Pd atoms were placed on second neighbor C–C bonds, because this configuration is the most stable in the case of parallel adsorption mode for the $Pd_2$ dimer (see Section 3.1). We considered for each complex both parallel and normal initial orientations to the SWCNT, as shown in Fig. 4. The geometrical parameters and OP values are reported in Table 6, as well as the binding energies computed from Equation (2) with $n = 2$. It can be seen that the most stable $H_2$ adsorption on the $Pd_2$/SWCNT system takes place in the Kubas-like complex G, which adopts a final geometry perpendicular to the nanotube with the H atoms located away from the surface (see Fig. 4h). Our calculations also show that the dihydrogen $Pd_2(H_2)$ isomer F is unstable on the SWCNT and relaxes to the complex G. The system E is adsorbed forming a $(PdH)_2$ rhomboid structure parallel to the nanotube surface (see Fig. 3g). This supported structure without an H–H bond involves a less stable $H_2$ adsorption than the Kubas-type complex. In contrast, the $H_2$ dissociation on the $Pd_2$ dimer is a more favored process in vacuum (see Table 1) and on graphene [21]. The different behavior on the nanotube can be explained if it is considered that the $Pd_2$ dimer is strongly adsorbed on a curved carbon surface and becomes less active for hydrogen dissociation. Therefore, we could conclude that the adsorption on the nanotube leads to a stabilization of the Kubas-type Pd–Pd($H_2$) complexes.

Our results in Tables 1 and 6 show that the H–H bond of the complex G is shortened 3.3% and strengthened 4.3% after interaction with the nanotube surface, while the Pd–H distances and overlaps are stretched 1.3% and weakened about 20%, respectively. At the same time, it can be seen from Tables 2 and 6 that when the hydrogen molecule is adsorbed on the Pd2 atom of the $Pd_2$/SWCNT system, the Pd1–Pd2 distance is increased 2.3% and the corresponding OP value is diminished 12.8%. C3–Pd2 and C4–Pd2 bonds are also weakened (up to 16.7%) after $H_2$ adsorption on the Pd2 atom, but the C1–Pd1 and C2–Pd1 OP values decrease less than 1.3%. As a result, the C3–C4 overlap is the shortest and strongest surface's bond in the Kubas-type $H_2$/$Pd_2$/SWCNT system (compare Table 2 vs. Table 6). On the other hand, the adsorption of the $(PdH)_2$ complex E on the nanotube is accompanied by noticeable elongation and weakening of the Pd–H bonds (until 5.1% and 31.5%, respectively, compare values in Tables 1 and 6). In this case, the Pd–Pd and C–Pd bonds are notoriously weakened (70.7% and up to 49.8%, respectively, see Tables 2 and 6) after $H_2$ dissociation on the nanotube-supported $Pd_2$ dimer. Simultaneously, C1–C2 and C3–C4 bonds, where the complex is adsorbed, are strengthened 3.0% and the C2–C3 OP value is augmented 4.8% (see Tables 2 and 6). It should be also noted from Table 6 that the hydrogen dissociative $(PdH)_2$/SWCNT system E has Pd–H bonds much stronger than those developed in the supported Kubas-type complex G, in which hydrogen remains in a molecular-like state. Accordingly, the Pd–Pd overlap is weaker in the coordination structure E adsorbed on the nanotube. Bonding analysis reported in our previous study on graphene [21] show that the $Pd_2H_2$ complexes adsorbed on a flat carbon surface involve weaker C–Pd and stronger Pd–H bonds than those of the corresponding $H_2$/$Pd_2$/SWCNT systems.

Finally, the Mulliken orbital populations given in Table 7 reveals that after $H_2$ dissociation on the $Pd_2$-decorated nanotube the C 2*s* orbitals are depopulated up to 1.2% and the electron occupancies of the C 2*p* orbitals are increased until 1.9%. (compare with Table 3). In this way, more limited donation and back-donation charge transfers are produced between $Pd_2$ and SWCNT in presence of hydrogen, and the C–Pd bonding results strongly weakened in the supported complex E. The changes in the electron densities of C 2*s* and 2*p* orbitals are smaller (up to −0.4% and 1.2%, respectively) for the nanotube-adsorbed Kubas-type complex G, indicating that a less important C–Pd weakening occurs when the hydrogen is molecularly adsorbed. Table 7 also shows that the H 1*s* orbitals of the complex E are less populated after adsorption on the nanotube (the electron occupation is 1.095 in vacuum), leading to weaker Pd–H overlaps than those found in gas-phase (see Table 1). The occupancy of the H 1*s* orbitals is 0.953 in the isolated complex G, so these orbitals increase its electron density after adsorption and the H–H bonding becomes stronger than in vacuum. We also computed the electron occupations of the hydrogen molecular orbitals for the nanotube-supported Kubas-type complex. The electron populations of the $H_2$ $\sigma$ and $\sigma^*$ orbitals are 1.903 and 0.030,

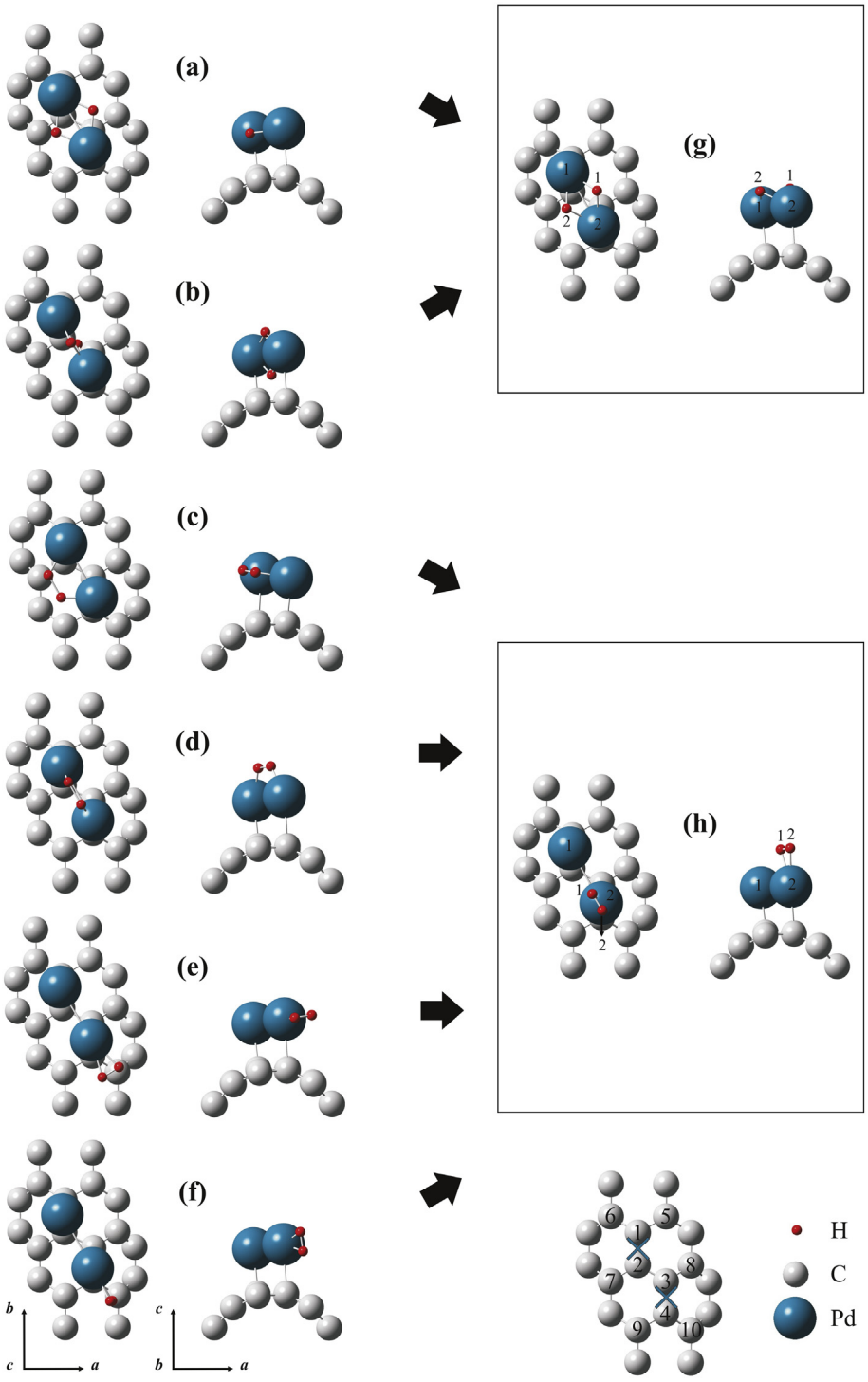


**Fig. 4 – Initial local adsorption geometries for the $H_2/Pd_2$/SWCNT systems. (a) Complex E parallel to the surface. (b) Complex E perpendicular to the surface. (c) Complex F parallel to the surface. (d) Complex F perpendicular to the surface. (e) Complex G parallel to the surface. (f) Complex G perpendicular to the surface. Final adsorption geometries (g and h) are also indicated.**

respectively, after adsorption. We can thus conclude that both the $\sigma$ donation and the $\pi$ back-donation are increased when a second Pd atom is adsorbed nearby the Pd($H_2$) Kubas system (compare with electron molecular orbital occupations in Section 3.2). Consequently, the Pd–H overlap in $Pd_2$($H_2$)/SWCNT is stronger than that in Pd($H_2$)/SWCNT. $H_2/Pd_2$/graphene systems presented analogous changes in their atomic orbital occupations [21], but C–Pd donation and back-donation delocalizations are much less pronounced that those originated on the nanotube. In the same way, the Kubas-type interactions between $Pd_2$ and $H_2$ in the graphene-supported complex G are higher that on the SWCNT [21].

**Table 6 – Distances (*d*), overlap populations (OP) and binding energies ($E_b$) for optimized $H_2/Pd_2$/SWCNT systems.[a]**

| Bond | $H_2/Pd_2$/SWCNT E (parallel to the surface) | | $H_2/Pd_2$/SWCNT G (perpendicular to the surface) | |
|---|---|---|---|---|
| | $E_b(H_2) = 0.37$ eV | | $E_b(H_2) = 0.67$ eV | |
| Enlace | *d* (Å) | OP | *d* (Å) | OP |
| C1–C2 | 1.436 | 0.999 | 1.449 | 0.971 |
| C3–C4 | 1.433 | 1.007 | 1.436 | 1.002 |
| C2–C3 | 1.463 | 0.939 | 1.476 | 0.909 |
| C1–C5 | 1.457 | 0.930 | 1.454 | 0.934 |
| C1–C6 | 1.448 | 0.949 | 1.452 | 0.940 |
| C2–C7 | 1.442 | 0.970 | 1.457 | 0.943 |
| C3–C8 | 1.442 | 0.971 | 1.448 | 0.962 |
| C4–C9 | 1.461 | 0.924 | 1.455 | 0.936 |
| C4–C10 | 1.451 | 0.948 | 1.452 | 0.946 |
| C1–Pd1 | 2.279 | 0.138 | 2.141 | 0.158 |
| C2–Pd1 | 2.364 | 0.076 | 2.187 | 0.139 |
| C3–Pd2 | 2.423 | 0.063 | 2.279 | 0.104 |
| C4–Pd2 | 2.326 | 0.126 | 2.210 | 0.131 |
| Pd1–Pd2 | 2.752 | 0.033 | 2.767 | 0.100 |
| Pd1–H1 | 1.765 | 0.221 | – | – |
| Pd1–H2 | 1.777 | 0.212 | – | – |
| Pd2–H1 | 1.752 | 0.230 | 1.765 | 0.082 |
| Pd2–H2 | 1.748 | 0.235 | 1.765 | 0.084 |
| H1–H2 | – | – | 0.846 | 0.738 |

[a] Binding energies were calculated according Eq. (2) with $n = 2$. Atom labeling is indicated in Fig. 4.

Our results suggest that the hydrogen adsorption on CNTs decorated with $Pd_2$ dimers produces preferably a Kubas-type Pd–Pd($H_2$) complex, in which the Pd–Pd bond is weaker than that of the $Pd_2$/SWCNT system. Therefore, it is reasonable to expect that the Pd–Pd overlap will also be weakened by a second $H_2$ molecule adsorbed on the hydrogen-free Pd atom of the supported complex G. We performed bonding analysis on a Kubas-type Pd($H_2$)–Pd($H_2$)/SWCNT system in order to verify this assumption. Our calculations show that the Pd–Pd OP value decreased about 20% when a second hydrogen molecule is adsorbed on the Pd–Pd($H_2$)/SWCNT system. This result suggests that the adsorption of multiple $H_2$ molecules could enhance the dissociation of the $Pd_2$ dimers supported on the SWCNT.

## 4. Conclusions

In this work we have examined by DFT calculations the molecular and dissociative adsorption of hydrogen on single Pd atoms and $Pd_2$ dimers adsorbed on a SWCNT. Several $PdH_2$ and $Pd_2H_2$ systems were considered. The main bonding interactions and atomic orbital contributions were described in all cases. Our results show that the most stable hydrogen adsorption on the Pd/SWCNT and $Pd_2$/SWCNT systems corresponds to Kubas-type dihydrogen complexes, in which the H–H bond is relaxed but not dissociated. Classic hydrides HPdH are unstable on the SWCNT. We also found that the $(PdH)_2$ complex, which is originated after $H_2$ dissociation on the nanotube-supported $Pd_2$ dimer, is less stable than the $Pd_2(H_2)$ Kubas-type complex. In contrast, the dissociative $(PdH)_2$ system is the most favored complex on graphene [21]. This different behavior can be attributed to the stronger interaction between the $Pd_2$ dimer and the curved SWCNT surface. We also verified that the Pd–Pd overlap in $H_2/Pd_2$/SWCNT Kubas-type systems is affected by two donor–acceptor delocalizations: (1) Pd 4*d* to C 2*s* donation and C 2*p* to Pd 5*s* back-donation; and (2) $H_2$ $\sigma$ to Pd 5*s* donation and Pd 4*d* to $H_2$ $\sigma^*$ back-donation. Our calculations suggest that the curvature of the CNTs improves the first interactions, limiting the palladium dimerization process. We expect that the presence of hydrogen facilitates even more atomization of the decoration. Therefore, a significative part of the palladium loading could exist atomically dispersed on real carbon supports, leading to an important hydrogen uptake based on Kubas-type bonding. Recent experimental evidence [18,19] supports our findings.

**Table 7 – Electron orbital occupations for optimized $H_2/Pd_2$/SWCNT systems.[a]**

| Atom | $H_2/Pd_2$/SWCNT E (parallel to the surface) | | | $H_2/Pd_2$/SWCNT G (perpendicular to the surface) | | |
|---|---|---|---|---|---|---|
| | *s* | *p* | *d* | *s* | *p* | *d* |
| C1 | 1.191 | 2.782 | – | 1.198 | 2.743 | – |
| C2 | 1.191 | 2.761 | – | 1.205 | 2.729 | – |
| C3 | 1.189 | 2.772 | – | 1.198 | 2.755 | – |
| C4 | 1.190 | 2.780 | – | 1.194 | 2.767 | – |
| C5 | 1.177 | 2.805 | – | 1.177 | 2.805 | – |
| C6 | 1.174 | 2.811 | – | 1.175 | 2.817 | – |
| C7 | 1.172 | 2.818 | – | 1.174 | 2.819 | – |
| C8 | 1.171 | 2.820 | – | 1.173 | 2.823 | – |
| C9 | 1.179 | 2.792 | – | 1.179 | 2.791 | – |
| C10 | 1.173 | 2.808 | – | 1.175 | 2.813 | – |
| Pd1 | 0.345 | 0.141 | 9.642 | 0.367 | 0.055 | 9.812 |
| Pd2 | 0.349 | 0.144 | 9.637 | 0.368 | 0.072 | 9.741 |
| H1 | 1.013 | – | – | 0.963 | – | – |
| H2 | 1.011 | – | – | 0.970 | – | – |

[a] Atom labeling is indicated in Fig. 4.

## Acknowledgments

The authors gratefully acknowledge the financial support of Universidad de Buenos Aires (CyT-UBA-20020110200044), SGCyT-UNS and ANPCyT (PICT 2011-1312 and 2010-1770). I.L.C. and A.J. are members of CONICET. The authors also acknowledge to the Departamento de Química and the Departamento de Física (UNS).

## REFERENCES

[1] Yürüma Y, Taralp A, Veziroglu TN. Storage of hydrogen in nanostructured carbon materials. Int J Hydrogen Energy 2009;34:3784–98.
[2] Yang RT, Wang Y. Catalyzed hydrogen spillover for hydrogen storage. J Am Chem Soc 2009;131:4224–6.
[3] Lachawiec AJ, Qi GS, Yang RT. Hydrogen storage in nanostructured carbons by spillover: bridge-building enhancement. Langmuir 2005;21:11418–24.
[4] Zacharia R, Kim KY, Fazle Kibria AKM, Nahm KS. Enhancement of hydrogen storage capacity of carbon nanotubes via spill-over from vanadium and palladium nanoparticles. Chem Phys Lett 2005;412:369–75.
[5] Yang FH, Lachawiec AJ, Yang RT. Adsorption of spillover hydrogen atoms on single-wall carbon nanotubes. J Phys Chem B 2006;110:6236–44.
[6] Zacharia R, Rather S, Hwang SW, Nahm KS. Spillover of physisorbed hydrogen from sputter-deposited arrays of platinum nanoparticles to multi-walled carbon nanotubes. Chem Phys Lett 2007;434:286–91.
[7] Bhat VV, Contescu CI, Gallego NC. The role of destabilization of palladium hydride in the hydrogen uptake of Pd-containing activated carbons. Nanotech 2009;20:204011.
[8] Kubas GJ. Molecular hydrogen complexes: coordination of a σ bond to transition metals. Acc Chem Res 1988;21:120–8.
[9] Phillips AB, Shivaram BS. High capacity hydrogen absorption in transition metal–ethylene complexes observed via nanogravimetry. Phys Rev Lett 2008;100:105505.
[10] Hamaed A, Trudeau M, Antonelli DM. $H_2$ storage materials (22 kJ/mol) using organometallic Ti fragments as σ-$H_2$ binding sites. J Am Chem Soc 2008;130:6992–9.
[11] Yildirim T, Ciraci S. Titanium-decorated carbon nanotubes as a potential high-capacity hydrogen storage medium. Phys Rev Lett 2005;94:175501.
[12] Dag S, Ozturk Y, Ciraci S, Yildirim T. Adsorption and dissociation of hydrogen molecules on bare and functionalized carbon nanotubes. Phys Rev B 2005;72:155404.
[13] Durgun E, Ciraci S, Yildirim T. Functionalization of carbon-based nanostructures with light transition-metal atoms for hydrogen storage. Phys Rev B 2008;77:85405.
[14] Xiao H, Li SH, Cao JX. First-principles study of Pd-decorated carbon nanotube for hydrogen storage. Chem Phys Lett 2009;483:111–4.
[15] Ströbel R, Garche J, Moseley PT, Jörissen L, Wolf G. Hydrogen storage by carbon materials. J Power Sources 2006;159:781–801.
[16] Sun Q, Wang Q, Jena P, Kawazoe Y. Clustering of Ti on a $C_{60}$ surface and its effect on hydrogen storage. J Am Chem Soc 2005;127:14582–3.
[17] Krasnov PO, Ding F, Singh AB, Yakobson BI. Clustering of Sc on SWNT and reduction of hydrogen uptake: ab-initio all-electron calculations. J Phys Chem C 2007;111:17977–80.
[18] Contescu CI, van Benthem K, Li S, Bonifacio CS, Pennycook SJ, Jena, et al. Single Pd atoms in activated carbon fibers and their contribution to hydrogen storage. Carbon 2011;49:4050–8.
[19] van Benthem K, Bonifacio CS, Contescu CI, Gallego NC, Pennycook SJ. STEM imaging of single Pd atoms in activated carbon fibers considered for hydrogen storage. Carbon 2011;49:4059–63.
[20] López-Corral I, Germán E, Juan A, Volpe MA, Brizuela GP. DFT study of hydrogen adsorption on palladium decorated graphene. J Phys Chem C 2011;115:4315–23.
[21] López-Corral I, Germán E, Juan A, Volpe MA, Brizuela GP. Hydrogen adsorption on palladium dimer decorated graphene: a bonding study. Int J Hydrogen Energy 2012;37:6653–65.
[22] Ordejón P, Artacho E, Soler JM. Self-consistent order-N density-functional calculations for very large systems. Phys Rev B 1996;53:R10441–4.
[23] Soler JM, Artacho E, Gale JD, García A, Junquera J, Ordejón P, et al. The SIESTA method for ab initio order-N materials simulation. J Phys: Condes Matter 2002;14:2745–79.
[24] Perdew JP, Burke K, Ernzerhof M. Generalized gradient approximation made simple. Phys Rev Lett 1996;77:3865–8.
[25] Junquera J, Paz O, Sánchez-Portal D, Artacho E. Numerical atomic orbitals for linear-scaling calculations. Phys Rev B 2001;64:235111.
[26] Troullier N, Martins JL. Efficient pseudopotentials for plane-wave calculations. Phys Rev B 1991;43:1993–2006.
[27] Hoffmann R. Solids and surfaces: a chemist's view of bonding in extended structures. New York: VCH Publ. Inc.; 1988.
[28] Landrum GA, Glassey WV. Yet another extended Hückel molecular orbital package (YAeHMOP). Ithaca: Cornell University Press; 2006. YAeHMOP is freely available on the world wide web at: http://yaehmop.sourceforge.net/.
[29] López-Corral I, Germán E, Volpe MA, Brizuela GP, Juan A. Tight-binding study of hydrogen adsorption on palladium decorated graphene and carbon nanotubes. Int J Hydrogen Energy 2010;35:2377–84.
[30] Monkhorst HJ, Pack JD. Special points for Brillouin-zone integrations. Phys Rev B 1976;13:5188–92.
[31] Durgun E, Dag S, Bagci VMK, Gülseren O, Yildirim T, Ciraci S. Systematic study of adsorption of single atoms on a carbon nanotube. Phys Rev B 2003;67:201401.
[32] Durgun E, Dag S, Ciraci S, Gülseren O. Energetics and electronic structures of individual atoms adsorbed on carbon nanotubes. J Phys Chem B 2004;108:575–82.
[33] Cabria I, Lopez MJ, Alonso JA. Theoretical study of the transition from planar to three-dimensional structures of palladium clusters supported on graphene. Phys Rev B 2010;81:035403.
[34] Thapa R, Sen D, Mitra MK, Chattopadhyay KK. Palladium atoms and its dimers adsorbed on graphene: first-principles study. Phys B 2011;406:368–73.
[35] Efremenko I, German ED, Sheintuch M. Density functional study of the interactions between dihydrogen and $Pd_n$ ($n$ = 1-4) clusters. J Phys Chem A 2000;104:8089–96.
[36] Ni MY, Zeng Z. Density functional study of hydrogen adsorption and dissociation on small $Pd_n$ ($n$ = 1-7) clusters. J Mol Struct: THEOCHEM 2009;910:14–9.
[37] Maiti A, Ricca A. Metal–nanotube interactions: binding energies and wetting properties. Chem Phys Lett 2004;395:7–11.
[38] Efremenko I, Sheintuch M. Carbon-supported palladium catalysts. Molecular orbital study. J Catal 2003;214:53–67.